Controlling spin-dependent tunneling by bandgap tuning in epitaxial rocksalt MgZnO films

D. L. Li,[1] Q. L. Ma,[1] S. G. Wang *,[1,†] R. C. C. Ward,[2] T. Hesjedal,[2] X.-G. Zhang,[3,4]
A. Kohn,[5] E. Amsellem,[5] G. Yang,[1] J. L. Liu,[1] J. Jiang,[1] H. X. Wei,[1] and X. F. Han[1]

[1]*State Key Laboratory of Magnetism, Beijing National Laboratory for Condensed Matter Physics, Institute of Physics, Chinese Academy of Sciences, Beijing 100190, China*

[2]*Clarendon Laboratory, Department of Physics, University of Oxford, Oxford OX1 3PU, UK*

[3]*Department of Physics and Quantum Theory Project, University of Florida, Gainesville, Florida 32611, USA*

[4]*Center for Nanophase Materials Sciences and Computer Science and Mathematics Division, Oak Ridge National Laboratory, Oak Ridge, Tennessee 37831-6493, USA*

[5]*Department of Materials Engineering, Ilse Katz Institute for Nanoscale Science and Technology, Ben-Gurion University of the Negev, Beer-Sheva 84105, Israel*

(Dated: November 4, 2014)

I. STRUCTURAL ANALYSIS

Epitaxial multilayers with a core structure of Fe(25)/$Mg_{1-x}Zn_xO$(3)/Fe(10)/IrMn(10) (in nm) were grown on single crystal MgO(001) substrates by MBE. The $Mg_{1-x}Zn_xO$ layer was grown by co-evaporation of MgO and Zn. The micrometer-sized tunnel junctions were fabricated by optical lithography combined with Ar-ion beam milling.

During deposition, each layer was monitored by *in situ* reflection high energy diffraction (RHEED). Figure S1 shows typical RHEED patterns recorded from Fe/$Mg_{1-x}Zn_xO$/Fe multilayers, where $x = 0$ (a), 0.15 (b), and 0.3 (c), respectively. The sharp and streaky RHEED patterns demonstrate high-quality epitaxial growth. With increasing Zn doping concentration, the RHEED patterns for the $Mg_{1-x}Zn_xO$ barrier remain streaky, however, the brightness and sharpness of the streaks get weaker for $x \geq 0.3$,

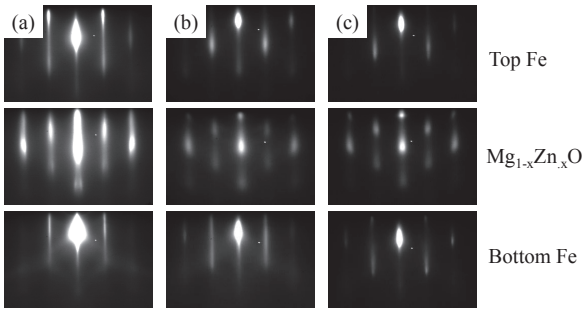

Figure S 1: RHEED patterns recorded along the MgO[110] direction for MTJ core layers with varying Zn concentration x. (**a-c**) for x=0, 0.15, and 0.3, respectively.

* Author to whom correspondence should be addressed. Email: sgwang@iphy.ac.cn

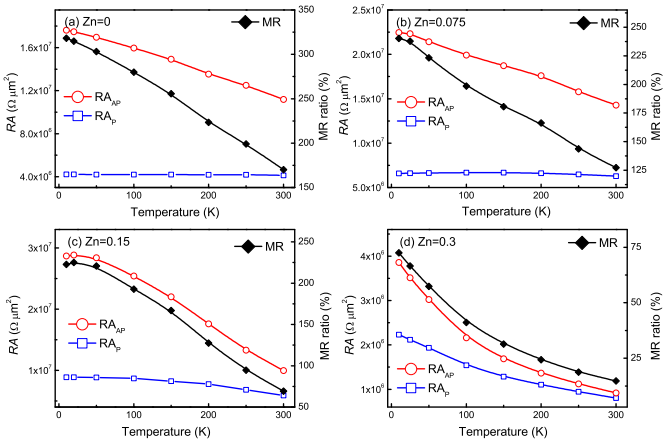

Figure S 2: Temperature dependence of $RA_{\mathrm{P,AP}}$ (right axis) and MR ratio (left axis) for varying x.(a-d) x=0, 0.075, 0.15, and =0.3, respectively. The open dots, squares, and diamonds are experimental data, and the solid line is a guide for the eyes only.

indicating that epitaxial growth is no longer possible owing to the large lattice mismatch between Fe and MgZnO layers.

The structure is further characterised by X-ray diffraction (XRD) although it is hard to distinguish the MgZnO barrier from MgO substrate due to its small thickness (3 nm) and epitaxial relationship. From the results of RHEED, XRD, and HRTEM, the epitaxial relationship of Fe(001)[100]‖MgZnO(001)[110]‖Fe(001)[100] is confirmed, where the MgZnO axes rotate 45° with respect to the equivalent Fe axes in order to have an epitaxial growth between MgZnO and Fe layers. Because the ionic radius of Zn^{2+} (0.83 Å) is larger than Mg^{2+} (0.78 Å), Zn incorporation into the cubic MgO lattice will enlarge the lattice constant. The structural transition from rocksalt to wurtzite takes place at about $x = 0.4$. The RHEED pattern for the $Mg_{0.6}Zn_{0.4}O$ barrier does not show clear and sharp streaks, and it exhibits polycrystalline rings instead of single crystal streaks for its top Fe layer. Furthermore, the junctions with $x = 0.4$ only show very low MR ratio at RT (less than 10%). Therefore, our focus was given on the junctions with $x \leq 0.3$ in this work.

Based on the microstructural analysis from RHEED, XRD, XPS and HRTEM, for multilayers with $x \leq 0.3$ the epitaxial relationship of Fe/MgZnO/Fe structures can be maintained where MgZnO layer shows a rocksalt structure.

II. TEMPERATURE DEPENDENCE

Figure S2 summarises typical results of the temperature dependence of the TMR ratio and $RA_{\mathrm{P,AP}}$. For $x = 0$ (Fe/MgO/Fe MTJs) shown in Figure S2(a), R_P is almost temperature independent, and R_{AP} shows an increase with decreasing temperature. This results in a great increase of TMR ratio with temperature, a characteristic for single crystal MgO barrier [1, 2]. For $x = 0.3$, shown in figure S2(d), both R_{P} and R_{AP} increase with decreasing temperature, a typical behavior for amorphous AlO_x-based junctions. With respect to R_{P}, it is nearly temperature independent for $x = 0$ and 0.075. With increasing Zn doping concentration, the dependence on temperature becomes more pronounced. The temperature dependence of TMR ratio changes greatly with varying x. For example, the TMR ratio increases nearly twice when the temperature decreases from RT to 10 K for $x = 0$ (172% at 300 K and 318% at 10 K, respectively). However, it shows a slight increases from 15% at 300 K to 75% at 10 K for $x = 0.3$, a much stronger temperature dependence. Obviously, the bandgap of Zn-doping in MgO barrier plays a dominant role on the transport of spin polarised electrons, leading to different temperature behaviour.

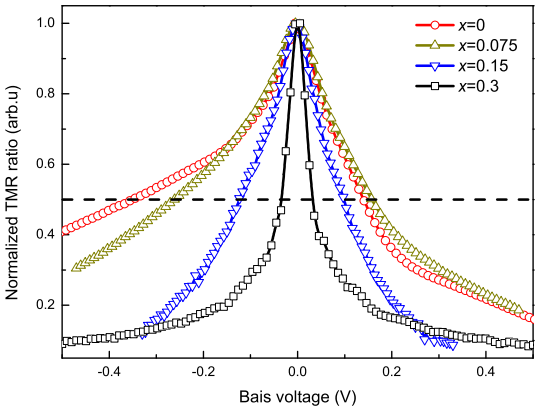

Figure S 3: Bias voltage dependence of normalised TMR ratio with various Zn-doping x. The dashed line indicates a TMR ratio of 50%.

Therefore, the bandgap tuned by Zn-doping into MgO barrier leads to different temperature behaviour, which is critical for industrial devices. It can be a valuable way to optimise the working parameters by tuning bandgap, such as TMR ratio, RA values and working temperature.

III. BIAS VOLTAGE DEPENDENCE

The TMR ratio shows a decrease with increasing bias voltage, and this behaviour severely affects the device performance as a bias is applied during device operation. This behaviour is quantified by $V_{1/2}$: the voltage at which the TMR ratio is half of the zero bias value. The normalised TMR ratio as a function of bias voltage with varying Zn-doping x is presented in Figure S3, where the dashed line is a guide for the eye only. Here, $V_{1/2}^{+}$ and $V_{1/2}^{-}$ is for positive and negative voltages at which the TMR ratio decreases to 50%, respectively. The value of $V_{1/2}$ is the average of $V_{1/2}^{+}$ and $V_{1/2}^{-}$. It can be seen that the value of $V_{1/2}^{-}$ decreases much more quickly than that of $V_{1/2}^{+}$. The asymmetry of dynamic conductance between positive and negative biases is more obvious for lower doping, which comes from the different interfacial structures [3, 4].

IV. BARRIER HEIGHT

In general, the barrier height in a tunnel junction can be estimated by Simmons formula, where the fitting is divided into low voltage and intermediate range, respectively [5, 6]. It is worthy to emphasise that the tunneling theory used to fit the $I-V$ curves was based on the tunnel junctions constituting of two nonmagnetic metallic electrodes separated by a thin insulating barrier. However, for magnetic tunnel junctions the $I-V$ behaviour between parallel and antiparallel configurations exhibits great difference because the interfacial structures across barrier are asymmetric. This asymmetry in MgO-based MTJs is significantly obvious, confirmed by the surface X-ray diffraction, X-ray photoelectron spectroscopy, and the inelastic electron tunneling spectroscopy (IETs) with the support of the first-principles calculation [3, 4, 7]. Here, a newly developed theory about the conductance in the magnetic tunnel junctions will be introduced where the asymmetry across the barrier is taken into account.

The simplest model for a tunneling barrier is that of a step potential for an incident-free electron. In a metal/insulator/metal tunnel junction, the insulator acts as a tunnel barrier because it has a bandgap around the Fermi energy of the metal. For electrons

the height of the tunnel barrier is how much the bottom of the conduction band of the insulating layer above the Fermi energy. If this energy difference is ϕ, then we can approximate the insulator by a step potential of height ϕ. When a bias voltage V is applied on the junction, the lowest order approximation is that the voltage drop is uniformly distributed across the tunnel barrier, so that the potential varies linearly with the position. Under these assumptions, we use the so-called Wenzel-Kramer-Brillouin (WKB) approximation of the quantum mechanical solution to obtain the current-voltage dependence for a simple step barrier. Within the WKB approximation, the transmission probability for an electron with incident energy E_z is proportional to the exponential factor,

$$T \propto \exp\left[-S\int_0^d dz\sqrt{U(z)-E_z}\right], \tag{1}$$

where $U(z) = \mu_L + \phi_1 + (\phi_2 - eV - \phi_1)z/d$, ϕ_1 and ϕ_2 are the barrier heights on the two interfaces measured from the zero bias Fermi energy μ, $S = 2\sqrt{2m^*}/\hbar$ with m^* being the effective mass of the tunneling electron, and d is the barrier thickness, respectively. The current density as a function of the applied bias voltage V can be calculated from Eq. (1).

We define $E_{xy} = E - E_z = \hbar^2 k_\parallel^2/2m^*$, and the current density is presented as:

$$J(V) = \frac{m^* e}{2\pi^2\hbar^3}\int_0^\infty dE\int_0^E dE_{xy}T(E_z)\left[f\left(E-\mu_L\right) - f\left(E-\mu_R\right)\right], \tag{2}$$

where we have used $\mu_R = \mu_L - eV$. The upper limit for E_{xy} is E because E_z cannot be negative in this model.

Using Eq. (1) to calculate the full $I-V$ curve is tedious. We first follow Simmons [5] and simplify Eq. (1) by replacing the integrand with an average $\mu_L + \phi_- - E_z$ where

$$\phi_\pm = \frac{\phi_1+\phi_2}{2} \pm \frac{eV}{2}. \tag{3}$$

The total current density is

$$\begin{aligned} J(V) \;=\; & \frac{m^* e}{2\pi^2\hbar^3}\int_0^\infty dE\int_0^E dE_{xy}\exp\left(-Sd\sqrt{\mu_L+\phi_- - E_z}\right) \\ & \left[f\left(E-\mu_L\right) - f\left(E-\mu_R\right)\right]. \end{aligned} \tag{4}$$

At $T = 0$ K this can be integrated to yield,

$$\begin{aligned} J(V) = \frac{e}{2\pi h d^2}\Bigg[& \left(\phi_- + \frac{3\sqrt{\phi_-}}{Sd} + \frac{3}{S^2d^2}\right)\exp\left(-Sd\sqrt{\phi_-}\right) \\ & - \left(\phi_+ + \frac{3\sqrt{\phi_+}}{Sd} + \frac{3}{S^2d^2}\right)\exp\left(-Sd\sqrt{\phi_+}\right)\Bigg]. \end{aligned} \tag{5}$$

When the higher order $1/(Sd\sqrt{\bar{\phi}})$ terms are neglected, this simplifies to the Simmons formula, that is often used to fit experimental current-voltage characteristics to extract useful information about tunnel barriers, such as barrier height and thickness. If we take the barrier thickness in nm, the barrier height in eV, and the applied voltage in V, then $S = 10.25\ \mathrm{eV}^{-1/2}\mathrm{nm}^{-1}$ and $e^2/2\pi h = 6.2\times10^8\ \mathrm{eV}^{-1}\mathrm{nm}^2$, and the resulting current density J is in the unit of $\mathrm{A/cm}^2$. In the past, the barrier thickness of

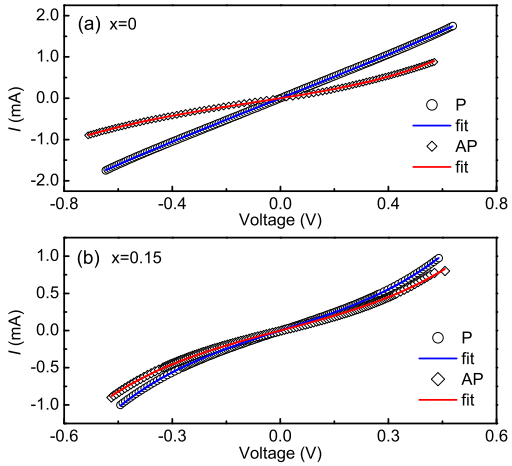

Figure S 4: $I-V$ **curves at 5 K and its fitting.** (**a**) for samples with x=0 and (**b**) with x=0.15. Here, open dots and diamonds are data for parallel and antiparallel configurations with their fit shown by solid lines, respectively.

a tunnel junction was often more than 10 nm and the barrier height was well over 1 eV, so the higher order $1/(Sd\sqrt{\bar{\phi}})$ terms can be safely neglected. But a typical magnetic tunnel junction consists of a barrier layer that approaches 1 nm, and the barrier height is usually not much over 1 eV. Therefore, the higher order terms can become significant.

Simmons derived his formula by replacing the integrand in Eq. (1) with an average barrier height. There are three effects that can cause a correction to the Simmons' formula. First, the applied bias effectively transforms the barrier shape from a square to a triangle. Second, the barrier height on both interfaces, ϕ_1 and ϕ_2, may not be the same, especially in MgO-based junctions which was discussed before. Third, there may be random fluctuations in the effective barrier height within the barrier due to defects. For this work we will account for the first two effects but neglect random fluctuations. We now re-evaluate the integral over z in Eq. (1) using $U(z) = \mu_L + \phi_1 + (\phi_2 - eV - \phi_1)z/d$ and obtain

$$\begin{aligned} & \frac{2d}{3(\phi_2 - eV - \phi_1)}\left[(\mu_L + \phi_2 - eV - E_z)^{3/2} - (\mu_L + \phi_1 - E_z)^{3/2}\right] \\ \approx\ & \sqrt{\mu_L + \phi_- - E_z}\,d - \frac{1}{96}\frac{(\phi_2 - eV - \phi_1)^2 d}{(\mu_L + \phi_- - E_z)^{3/2}} \\ \approx\ & \sqrt{\frac{\mu_L + \bar{\phi} - E_z}{1 + \dfrac{D}{48\bar{\phi}^2}}}\,d, \end{aligned} \tag{6}$$

where

$$D = (\phi_2 - eV - \phi_1)^2 . \tag{7}$$

and we used the expansion near $E_z = \mu_L - eV/2$ for which the tunneling current is the maximum. The current density with the

corrections is,

$$J(V) = \frac{e}{2\pi h d^2}\left(1+\frac{D}{48\bar{\phi}^2}\right)\left[\left(\phi_- + \frac{3\sqrt{\phi_-}}{S'd} + \frac{3}{(S'd)^2}\right)\exp\left(-S'd\sqrt{\phi_-}\right) - \left(\phi_+ + \frac{3\sqrt{\phi_+}}{S'd} + \frac{3}{(S'd)^2}\right)\exp\left(-S'd\sqrt{\phi_+}\right)\right]. \quad (8)$$

where

$$\phi_\pm = \bar{\phi} \pm \frac{eV}{2}, \quad (9)$$

and

$$S' = \frac{S}{\sqrt{1+\frac{D}{48\bar{\phi}^2}}} \quad (10)$$

The typical results of $I-V$ fitting by Eq. (8) were presented in Figure S4 for $x = 0$ and 0.15, respectively. The average value of barrier height as a function of Zn-doping x was shown in Figure 2(b, c). It can be clearly seen that the barrier height deceases gradually with increasing x, another powerful proof of the tunable bandgap of Zn-doped MgO layer.

† Electronic address: Sgwang@iphy.ac.cn

References

[1] Wang, S. G., Ward, R. C. C., Du, G. X., Han, X. F., Wang, C. & Kohn, A. Temperature dependence of giant tunnel magnetoresistance in epitaxial Fe/MgO/Fe magnetic tunnel junctions. *Phys. Rev. B* **78**, 180411R (2008).

[2] Yuasa, S., Fukushima, A., Kubota, H., Suzuki, Y. & Ando, K. Giant tunneling magnetoresistance up to 410% at room temperature in fully epitaxial Co/MgO/Co magnetic tunnel junctions with bcc Co(001) electrodes. *Appl. Phys. Lett.* **89**, 042505 (2005).

[3] Du, G. X., Wang, S. G., Ma, Q. L., Wang, Y., Ward, R. C. C., Zhang, X. -G., Wang, C., Kohn, A. & Han, X. F. Spin-dependent tunneling spectroscopy for interface characterization of epitaxial Fe/MgO/Fe magnetic tunnel junctions. *Phys. Rev. B* **81**, 064438 (2010).

[4] Wang, S. G., Ward, R. C. C., Hesjedal, T., Zhang, X. -G., Wang, C., Kohn, A., Ma, Q. L., Zhang, J., Liu, H. F. & Han, X. F. Interface characterization of epitaxial Fe/MgO/Fe magnetic tunnel junctions. *J. Nanosci. Nanotechnol.* **12**, 1006-1023 (2012).

[5] Simmons, J. G. Generalized formula for the electric tunnel effect between similar electrodes separated by a thin insulating film. *J. Appl. Phys.* **34**, 1793-1803 (1963).

[6] Simmons, J. G. Electric tunnel effect between dissimilar electrodes separated by a thin insulating film. *J. Appl. Phys.* **34**, 2851-2890 (1963).

[7] Meyerheim, H. L., Popescu, R., Kirschner, J., Jedrecy, N., Sauvage-Simkin, M., Heinrich, B. & Pinchaux, R. Geometrical and compositional structure at metal-oxide interfaces: MgO on Fe(001). *Phys. Rev. Lett.* **87**, 076102 (2001).